Journal of Statistical Physics, Vol. 39, Nos. 5/6, 1985

Numerical Simulation of Ion Acoustic Turbulence

E. L. Lindman[1]

Extensive simulation studies of ion acoustic turbulence carried out at the Max Planck Institute and at the Los Alamos National Laboratory are compared. Simulations of the $B = 0$ case carried out at the two laboratories agree when the Sagdeev scaling law without the T_e/T_i dependence is used to compare them. Typical results are shown. The level of turbulence is found to be quite high in spite of the low anomalous collision frequency. The role of the "differential drift" distribution in these simulations is discussed extensively.

KEY WORDS: Ion-acoustic waves; turbulence; plasma instability; plasma simulation; particle-in-cell calculation.

1. INTRODUCTION

Over the past 20 years considerable effort has been put into the study of ion acoustic turbulence[1-14] using plasma simulation techniques.[15] From this work much has been learned about numerical techniques for simulating collisionless plasma and ion acoustic turbulence. And, using the best of these techniques, considerable insight into certain aspects of ion acoustic turbulence have been gained. Nevertheless the numerical constraints imposed by machines, even today, suggest that the results obtained from these techniques should be used with caution. Indeed, M. G. Haines suggests that a fully satisfactory simulation would take about 1000 days of CDC 7600 time.[16] Many of us believe, however, that although such a calculation would be far more convincing, its results would be quite similar to the results already obtained.

Perhaps the most comprehensive set of such calculations[4,5,7,9,10] was carried out at the Max Planck Institute by Biskamp, Chodura, Dum, Von Hagenow, and Welter between 1970 and 1974. They performed two- and

[1] Los Alamos National Laboratory, Los Alamos, New Mexico 87545.

0022-4715/85/0600-0769$04.50/0

three-dimensional simulations, using standard PIC techniques[15] with mass ratios between 100 and 1600. All possible orientations of the current with respect to B were done in two dimensions: $B=0$; J parallel to B; J perpendicular to B with B out of the plane of the simulation; and J perpendicular to B with B in the plane of the simulation. The emphasis, however, was on the J perpendicular to B studies which apply to shock waves in magnetized plasmas.

Then, in 1975, concern about possible effects on the penetration of the thermal wave in laser–pellet interaction experiments[17] led to an extensive study of the $B=0$ case at Los Alamos by Forslund, Kindel, Lee, Lindman, and Morse. The primary result of these simulations was the lowest predicted anomalous resistivity of any theory or simulation at the time. As a result the work was not published until much later,[11] and then only as part of a review paper.

Theoretical calculations of the anomalous collision frequency have generally given values higher than those from simulation. An extensive review of the methods used, the results, and comparisons with simulation and experiment can be found in a comprehensive review paper by Horton and Choi.[18] In most such comparisons the cross-field simulations have been used exclusively. Here we will concentrate on the $B=0$ case.

2. COMPARISON OF LOS ALAMOS AND MPI METHODS

In the Los Alamos simulations the trajectories of 7.2×10^5 ions and 7.2×10^5 electrons were integrated in time using Newton's law:

$$M\ddot{\mathbf{X}} = Q(\mathbf{E}_0 - \nabla\phi) \tag{1}$$

At each time step the charge density was accumulated on a 64×64 mesh, whose dimensions were $32\lambda_D\times32\lambda_D$, using standard charge sharing methods.[15] A discrete smoothing operation was then used to enhance the accuracy in the physically accurate region of k space and to reduce the fluctuations in the high-k region which is physically inaccurate and contributes to unwanted numerical collisions. The electrostatic potential corresponding to this charge density was then obtained on the mesh by solving Poisson's equation with periodic boundary conditions in both x and y:

$$\nabla^2\phi = -4\pi(Q_i n_i + Q_e n_e) \tag{2}$$

An additional electric field which is constant in x and y was added to hold the total current constant in time. The instantaneous value of this electric field was determined by requiring that the sum of the displacement current

and the total conduction current be equal to a fixed value, J_0, usually held constant in time.

$$\dot{\mathbf{E}}_0 + 4\pi \sum Q\mathbf{V} = 4\pi \mathbf{J}_0 \tag{3}$$

As indicated above, the total conduction current is most easily obtained by summing the currents from all the particles in the system, ignoring their positions. This equation was then integrated in time to obtain E_0, and the combined electric field was then used to update the particle velocities using the standard force interpolation procedure.[15]

The simulations of Biskamp and Chodura[4,5] were done in a similar manner with a few exceptions. First, they did not use the additional k-space smoothing mentioned above, and second, they used a slightly different procedure for maintaining constant current. Probably the most important differences were the use of a 128×128 mesh whose physical dimensions were $51.2\lambda_D$ by $51.2\lambda_D$ and the use of only 2×10^5 ions and 2×10^5 electrons.

In particular, Biskamp and Chodura's choice of mesh parameters leads to a better k space coverage than ours. A comparison of the two, in Fig. 1, shows 1.6 times as many k's per unit length in k space for the MPI parameters compared to the Los Alamos runs, and 2.56 times as many per unit area. Although no one has done a careful calculation of the effects of discrete modes on ion acoustic turbulence, there is considerable concern that discreteness in k space may lead to nonnegligible errors. If so, more closely spaced k's should give a more accurate result.

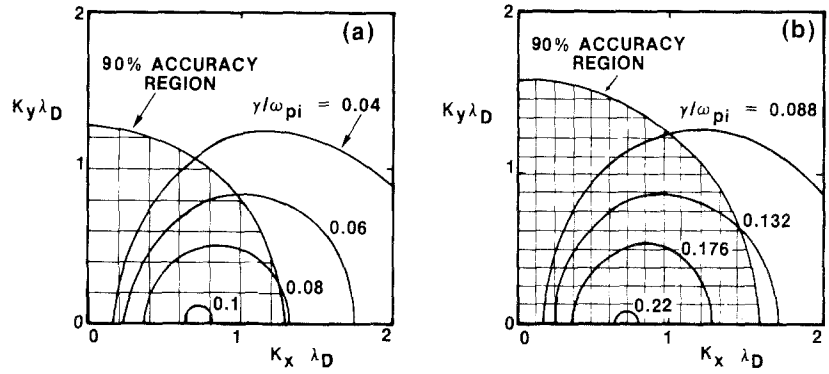

Fig. 1. Mode structure in simulations compared to initial growth rates. The discrete k values in the simulations occur at the intersections of the horizontal and vertical lines. For the Los Alamos simulations (a) the parameters are $V_D/V_{Te} = 0.5$, $M_i/M_e = 100$, $T_i/T_e = 0.01$, $N_x = N_y = 64$, $\Delta x = \Delta y = 0.5\lambda_D$; and for the MPI simulations (b) the parameters are: $V_D/V_{Te} = 1.0$, $M_i/M_e = 100$, $T_i/T_e = 0.02$, $N_x = N_y = 128$, $\Delta x = \Delta y = 0.4\lambda_D$.

On the other hand our choice of parameters leads to a substantially reduced collision frequency. Using the formulas given by Okuda and Birdsall[19] we may estimate the numerical collision frequencies in the two cases. For the Max Planck Institute,

$$\frac{\nu}{\omega_{pe}} = \frac{c(\alpha)}{16}\frac{1}{n\lambda_D^2} = \frac{0.5}{16}\frac{(51.2)^2}{2\times 10^5} = 4\times 10^{-4} \tag{4}$$

and for Los Alamos,

$$\frac{\nu}{\omega_{pe}} = \frac{c(\alpha)}{16}\frac{1}{n\lambda_D^2} = \frac{0.1}{16}\frac{(32)^2}{7\times 10^5} = 9\times 10^{-6} \tag{5}$$

These estimates may be verified by looking at the diagnostic that measures resistance early in the runs before the turbulence builds up. The Los Alamos value is quite negligible compared to the measured anomalous resistance value, whereas the MPI value is not negligible at late times. It has been argued that accurate anomalous collision frequencies could not be obtained from these calculations at late times for this reason.

Questions as to which approach gave the better answer are irrelevant, however, since the results of the two approaches will be shown to be essentially the same. This conclusion is an important one since it lends credence to calculations which use less computer time and shows that varying the discreteness does not affect the result. The unlikely situation in which the two effects canceled will be dealt with in a future paper.

4. TYPICAL RESULTS FOR THE $B=0$ CASE

The energy in the electric field normalized to the initial particle energy is shown in Fig. 2a. Because of the low initial fluctuation level, the energy in the field rises more than two decades before saturating. After saturation the field energy drops slowly. Similar data for the MPI calculations is shown in Fig. 2a of Ref. 5. Because of the higher noise level in the MPI calculation the field energy rises only one one decade before saturating at a value approximately twice that shown in Fig. 2. The difference in the saturation levels results from our choice of an electron drift velocity of 1/2 the thermal speed instead of Biskamp's choice of $V_D/V_{Te}=1$.

A similar factor of 2 is seen in the comparison of the anomalous resistance caused by the turbulence in the two calculations. This resistance can be obtained directly by monitoring the spatially constant ($k=0$) component of the electric field required to keep the current constant. A plot of this field strength as a function of time is shown in Fig. 2b. Large-

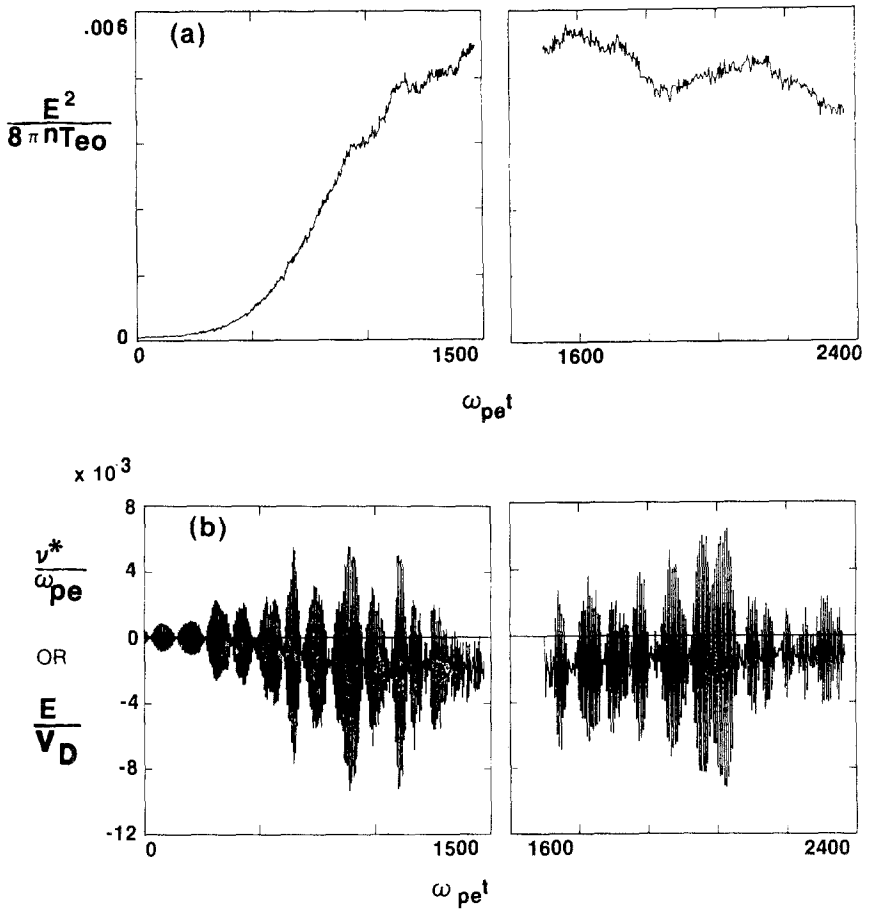

Fig. 2. Electric field energy density and anomalous collision frequency as a function of time. The energy in the electrostatic field of the ion acoustic waves normalized to the initial particle energy density is plotted for the duration of the simulation run in (a). The $k=0$ electric field required to hold the total current constant is plotted vs. time in (b). The high-frequency oscillations are plasma oscillations. The time average part of the curve is a direct measure of the anomalous collision frequency experienced by the electrons as they move through the ion acoustic turbulence.

amplitude plasma oscillations are seen superimposed on the field strength that varies with the resistivity. The plasma oscillations appear quite large here but the oscillating velocity of the electrons in them is small compared to their drift velocity, and hence they are unimportant. A detailed comparison of the collision frequencies seen in the two calculation will be presented later.

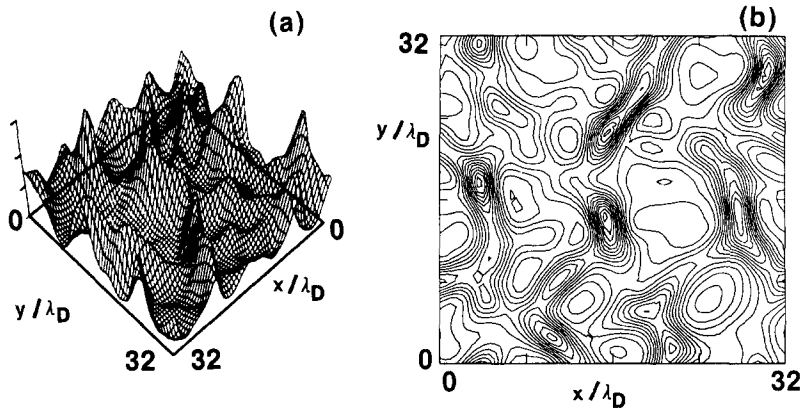

Fig. 3. Density fluctuations in real space. The ion density at $\omega_{pe}t = 1500$ is plotted as a function of x and y in (a); and a contour plot of similar data slightly displaced in time is presented in (b). The ion density ranges from $\delta n/n = -0.4$ to $+0.9$ with an rms value of 0.25 at which time it is at the peak of the turbulence level.

The rms value of the ion density fluctuations, $\delta n/n$, follows a curve qualitatively similar to that of the electric field energy in time. Near the peak of the curve, at $\omega_{pe}t \cong 1500$, a rms value of about 0.25 is obtained. At the same time a maximum value of 0.9 and a minimum value of -0.4 is seen. The fluctuation pattern corresponding to these data is shown in Fig. 3, and the wave spectrum is shown in Fig. 4. The spectrum is centered on the region in k space of maximum growth, $k_x\lambda_{De} \cong 0.7$, as expected.

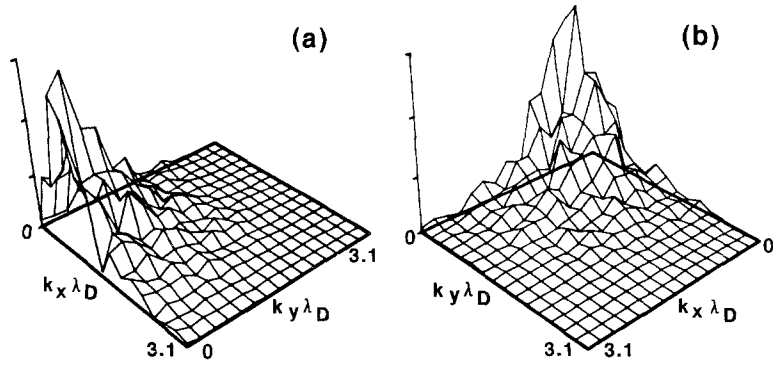

Fig. 4. Density fluctuations in k space. The absolute value of the Fourier transform of the density fluctuations is plotted as a function of k_x and k_y at $\omega_{pe}t = 1500$. The peak of the spectrum occurs near $k_x\lambda_D = 0.7$ which is consistent with the linear growth rate curves given in Fig. 1a.

The amplitudes of the ion density fluctuations in this simulation suggest that nonlinear wave effects may be important. The fact that the density minima tend to be broad while the density maxima tend to be sharp lends further support to this supposition. Although an expansion of the turbulence in plane waves predicts many of the observed effects, it may be that an expansion in terms of solitons, for instance, might prove superior. Certainly, much progress has been made recently in Langmuir turbulence using this approach.

Perhaps, the most important effect in the saturation of the instability is ion trapping as noted by Biskamp and Chodura. They included plots of the ion distriution function in their early work which shows the high-energy "tail" generated by this effect (Fig. 8 of Ref. 5). Figure 5 shows the same effect obtained in the Los Alamos simulation.

The hot ion "tail" is caused by the two-dimensional equivalence of wave breaking or trapping. The collection of waves previously discussed as ion density perturbations were generated by the ion acoustic instability in a cone of angles centered on the x axis. The interaction of these waves creates density structures moving at a wide variety of speeds and angles. These structures are capable of accelerating particles to high velocities in much the same way that particles are accelerated in wave breaking or trapping models. The distribution generated extends out to $2C_s$ in the x direction and almost as far in y. The deformation of the "bulk" ions is caused by the

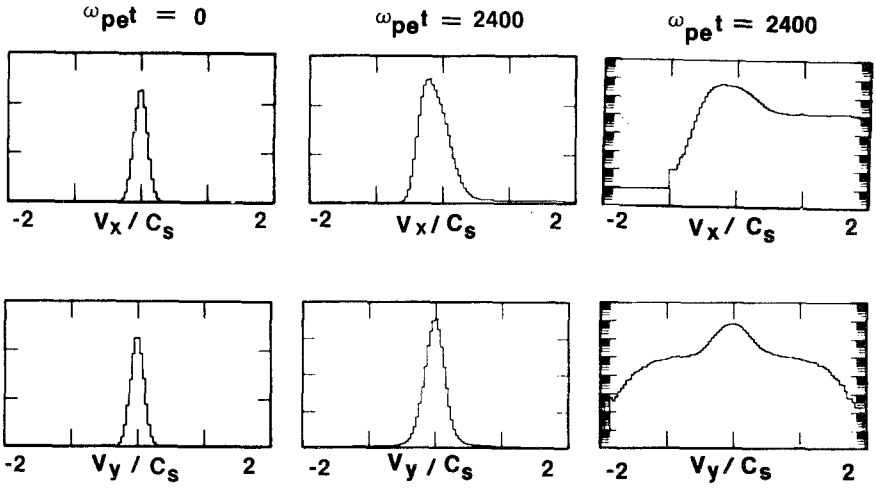

Fig. 5. Ion velocity distribution. The distribution of x velocities of the ions at $\omega_{pe}t = 0$ and $\omega_{pe}t = 2400$ is plotted. The hot ion tail is barely visible in the linear plot. The log-linear plot of the same data shows it quite clearly. The distribution of y velocities is also shown at equivalent times. The hot ion tail is visible here also and extends out to $V_y = \pm C_s$.

wave motion plus conservation of momentum for the ions as a whole during the formation of the hot "tail."

The distribution function of the electrons is also deformed but in a different way. This effect is shown in Fig. 6 (and in Fig. 7 of Ref. 5). At $t=0$ the electron distribution was initialized as a Maxwellian centered on the drift velocity. As the ion acoustic waves grow the electric fields associated with them scatter the electrons more effectively. Interestingly enough the velocity dependence of the scattering by these turbulent fields is exactly the same as that for Coulomb scattering. Thus we may analyze the effect on the distribution function of the scattering by these fields in exactly the same way as we analyze a distribution of electrons being dragged through a collection of Coulomb scattering centers[20] with velocities large compared to the scattering-center velocities. To lowest order the electron distribution should be at rest in the scattering-center frame. The effect of the applied $k=0$ field, E_0, however, is to drag the electrons through the scattering centers at a rate required to maintain the desire current. Assuming a zero-order stationary Maxwellian we have

$$f = f_0 + f_1 \tag{6}$$

$$f_0 = n_0(2\pi)^{-3/2} V_{\mathrm{Te}}^{-3} \exp[-V^2/(2V_{\mathrm{Te}}^2)] \tag{7}$$

$$f_1 = \frac{eE_0}{mv}\frac{\partial f_0}{\partial V_x} \tag{8}$$

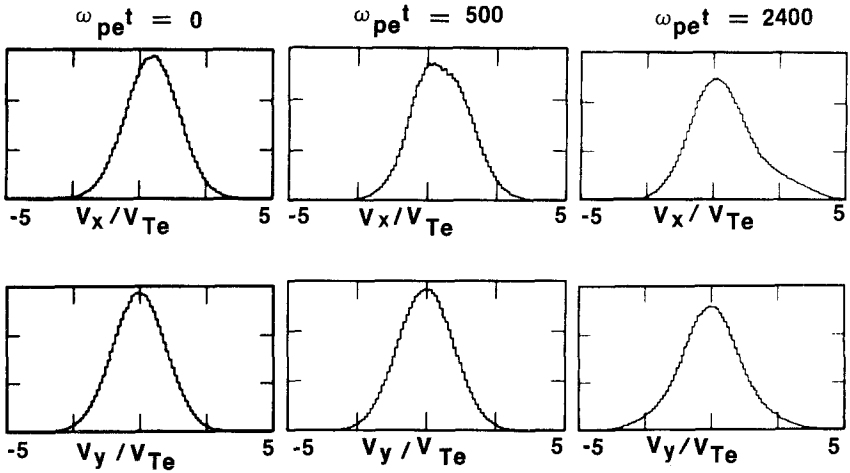

Fig. 6. Electron velocity distribution. The distribution of x velocities of the electrons at various times are shown. The initialized drifting Maxwellian is seen at $\omega_{\mathrm{pe}}t=0$. At $\omega_{\mathrm{pe}}t=200$ approximate "plateau" formation for $0 \leqslant V_x \leqslant C_s$ is seen. At late times the distribution becomes a differential mobility distribution with a maximum at approximately $0.3V_d$. In the y direction some heating is observed at late times.

To include the velocity dependence of ν, it is convenient to rewrite it as follows:

$$\nu = \nu_0 (V_{\mathrm{Te}}^3 / V^3) \tag{9}$$

If we now let $V_0 = -eE_0/(m\nu_0)$, the electron density, the current, and $f(V_x)$ may be computed from the distribution function as follows:

$$n = n_0 \tag{10}$$

$$J = -neV_d = 16\left(\frac{2}{\pi}\right)^{1/2} n_0 e V_0 \tag{11}$$

$$f(V_x) = 2\pi \int_0^\infty V_\perp \, dV_\perp \, f(V_\perp, V_x) \tag{12}$$

$$f(V_x) = (2\pi)^{-1/2} V_{\mathrm{Te}}^{-1} n_0 \exp[-V_x^2/(2V_{\mathrm{Te}}^2)] \times \left[1 + \frac{V_0 V_x^3 |V_x|^3}{2V_{\mathrm{Te}}^7} U\left(1, \frac{7}{2}; \frac{V_x^2}{2V_{\mathrm{Te}}^2}\right)\right] \tag{13}$$

where $U(a, b; x)$ is a confluent hypergeometric function.[21] Using the small argument expansion,

$$U(a, b; x) = \frac{\Gamma(b-1)}{\Gamma(a)} x^{1-b} + O(|x|^{b-2}) \tag{14}$$

we may obtain an approximate expression for $f(V_x)$ for $|V_x| \ll V_{\mathrm{Te}}$:

$$f(V_x) \cong (2\pi)^{1/2} V_{\mathrm{Te}}^{-1} n_0 \left[1 - \frac{9\pi}{4}\left(\frac{V_0}{V_{\mathrm{Te}}}\right)^2 + \left(\frac{V_x}{2^{1/2} V_{\mathrm{Te}}} - \frac{3\pi^{1/2}}{2}\frac{V_0}{V_{\mathrm{Te}}}\right)^2 + \cdots\right] \tag{15}$$

And the maximum of this distribution is located at

$$V_x = V_d' = 3\left(\frac{\pi}{2}\right)^{1/2} V_0 \tag{16}$$

which is less than drift velocity, V_d, of the original Maxwellian carrying the same current by a factor of ~ 0.3:

$$V_d' = \frac{3\pi^{1/2}}{32} V_d \cong 0.3 V_d \tag{17}$$

All the electrons are being dragged through the scattering centers by the same field, but the more energetic electrons have a weaker interaction

with the waves and, hence, drift faster. This *differential mobility* leads to the skewed distribution function shown in Fig. 5. Since the more energetic electrons are more mobile they carry more than their share of the current. The colder ones are less mobile and carry less current. As a result, the maximum in the distribution occurs at an x velocity which is smaller than that for a drifting Maxwellian carrying the same current. It is interesting to note that the shape of the distribution is not a function of the level of the turbulence in a constant current situation. The current is proportional to V_0 which is proportional to E_0/v_0. Thus as v_0 rises, E_0 rises with it to keep the current and, hence, V_0 constant. Since the distribution function is a function of v_0 only through V_0, it is independent of the turbulence level.

Therefore, there is a canonical distribution function that should be used in simulations of ion acoustic turbulence for $B=0$. The simulations done in the past were initialized with a drifting Maxwellian with all simulation parameters chosen to put the unstable k spectrum in the optimum location in k space. As the distribution function changed, however, the unstable modes were no longer located at the optimum and questionable results have been obtained for late times. In future simulations the differential-mobility distribution function for the electrons should be used in place of the drifting Maxwellian.

4. PARAMETRIC DEPENDENCIES

In order to compare the results of a number of dissimilar experiments or, in our case, simulations, it is convenient to compare to a scaling formula. Perhaps the best known of these is that proposed by R. Z. Sagdeev:

$$\frac{\nu^*}{\omega_{\mathrm{pe}}} = \alpha \frac{V_d}{V_{\mathrm{Te}}} \frac{T_e}{T_i} \left(\frac{m_e}{m_i}\right)^{1/4} \tag{18}$$

A number of simulations have been done at the Max Planck Institute and Los Alamos to check the dependences indicated above. Figure 7 shows the data that were originally published in the review article, Ref. 11. The 1/4 power dependence on the mass ratio is well established from these data, and Ref. 5 contains a table of data which also supports it. The two points at different temperature ratios and the same mass ratio appear to support the linear scaling with T_e/T_i. The conclusion is probably incorrect, however. Since the value of the electron temperature determines both the Debye length and, with the mass ratio, the sound speed, the temperature ratio is varied by varying the ion temperature, T_i. For $T_i/T_e \lesssim 0.05$ the linear dispersion relation for unstable ion acoustic waves goes to the cold ion limit. Thus from linear theory we expect no T_e/T_i scaling for $T_e/T_i \lesssim 20$.

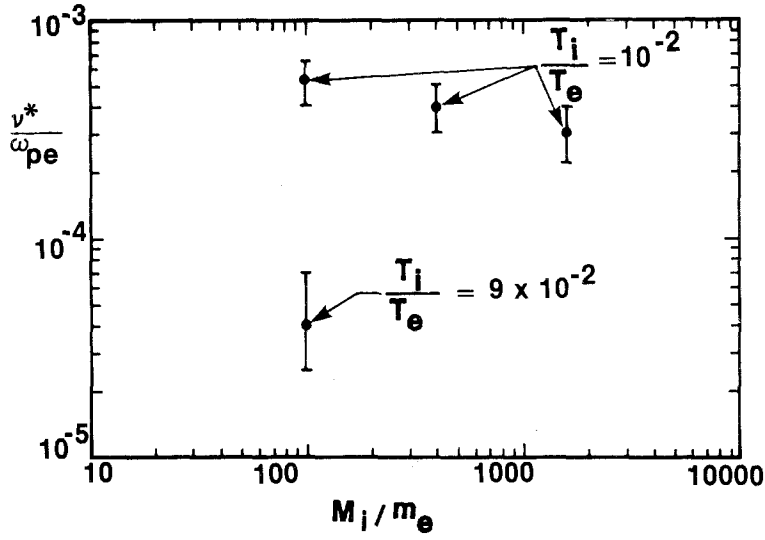

Fig. 7. Anomalous collision frequency vs. mass ratio. Anomalous collision frequencies are taken from simulations using mass ratios of 100, 400, and 1600. The $(M_i/M_e)^{-1/4}$ dependence is clearly established. The point at $M_i/M_e = 100$ and $T_i/T_e = 9 \times 10^{-2}$ shows a substantial decrease in anomalous collision frequency for warm ions.

The condition for ion trapping behaves similarly. It is dependent on the ion thermal velocity divided by the wave speed, $(T_i/m_i)^{1/2}(m_i/T_e)^{1/2}$. Thus, for $T_i/T_e \ll 1$, the ion temperature drops out of the ion-trapping condition.

Thus in the range $20 \leqslant T_e/T_i \leqslant \infty$, the linear scaling given above is questionable and, in fact, no scaling with temperature in the cold ion limit is probably correct. For $T_e/T_i \leqslant 20$ a much stronger dependence on T_e/T_i is expected consistent with the data shown in Fig. 5.

No one has published simulation data which verify the V_d/V_{Te} scaling. On the other hand the simulations published by the MPI group were all done at $V_d/V_{\mathrm{Te}} = 1$, whereas the work at Los Alamos was done at $V_d/V_{\mathrm{Te}} = 0.5$. Comparison of the results obtained at the two Laboratories may be used to check this scaling provided other differences, such as the number of particles used in the simulations, etc., can be neglected. Such a comparison is presented in Table I.

For the $B = 0$ case, agreement between the Los Alamos and the Max Planck results is quite good, if the T_e/T_i scaling in the Sagdeev scaling law is suppressed, as we have argued it should be for $T_e/T_i > 20$. In order to make this comparison it was assumed that the observed collision frequency in each simulation was simply the sum of the numerical collision frequency plus the anomalous collision frequency, and, hence the numerical collision

Table I. Comparison of Anomalous Collision Frequencies Obtained from Simulation[a]

	$\frac{\nu^* - \nu_0}{\omega_{pe}}$	$\frac{\nu^* - \nu_0}{\omega_{pe}\frac{V_d}{V_{Te}}\frac{T_e}{T_i}\left(\frac{M_e}{M_i}\right)^{1/4}}$	$\frac{\nu^* - \nu_0}{\omega_{pe}\frac{V_d}{V_{Te}}\left(\frac{M_e}{M_i}\right)^{1/4}}$
Biskamp and Chodura $\frac{T_e}{T_i}=50,\quad \frac{V_d}{V_{Te}}=1,\quad \frac{M_i}{M_e}=400$	8.4×10^{-4} (late time)	7.5×10^{-5}	3.7×10^{-3}
Los Alamos $\frac{T_e}{T_i}=100,\quad \frac{V_d}{V_{Te}}=0.5,\quad \frac{M_i}{M_e}=400$	4.0×10^{-4} (late time)	3.5×10^{-5}	3.5×10^{-3}
$B=0$	2.5×10^{-3} (at peaks)	Biskamp and Chodura	
$J_x \parallel B_{y0}$	2.6×10^{-3} (at peak)		
$J_x \sim E_{y0}\times B_{z0}$	4.3×10^{-3} (at peak)		
$J_x \sim E_{z0}\times B_{y0}$	1.6×10^{-2} (at peak)		

[a] The first two rows compare the $B=0$ simulations carried out at Los Alamos and the Max Planck Institute. Agreement is quite good when the Sagdeev scaling law is used and the T_e/T_i dependence is omitted. The bottom 4 entries show the anomalous collision frequencies obtained for different orientations of magnetic field. The cross-field cases are clearly higher and should not be compared with the $B=0$ and $J \parallel B$ cases.

frequency could be conveniently subtracted out. Since a steady state collision frequency is of most interest, the values were taken at late times in the simulations. The collision frequencies were still dropping at this time; hence, these values are at best upper bounds. Failure to set up the problems consistent with a differential-mobility electron distribution also casts doubt on the late time results. Nevertheless the simulations predict a very low anomalous collision frequency for the $B=0$ case.

When the current is maintained by causing the electrons to drift across a magnetic field, much stronger anomalous collision frequencies are obtained. In a two-dimensional simulation there are two ways to cause the electrons to $E\times B$ drift in the x direction. Both of them give higher anomalous collision frequencies than the J parallel to B case as shown in Table I. Where the mass ratio dependence has been determined it is no longer $(m_i/m_e)^{1/4}$. Furthermore, these cases give significantly different values for the anomalous resistance. Much of the confusion over the anomalous collision frequency associated with ion acoustic turbulence has occurred because of a desire to place all these cases in the same category.

5. CONCLUSION

The earliest in-depth simulation studies of ion acoustic turbulence were carried out by Biskamp, Chodura, Dum, Von Hagenow, and Welter between 1970 and 1974. The more recent simulation studies at Los Alamos by Forslund, Kindel, Lee, Lindman, and Morse appeared to disagree with the earlier work. The alleged discrepancy arose because (1) $B=0$ simulations at Los Alamos were compared with $E\times B$ driven simulations of MPI and (2) the T_e/T_i factor was retained in the scaling law in spite of the fact that both sets of simulations were done in the cold-ion limit. When only $B=0$ simulations are compared and a scaling law is used that has no T_e/T_i factor, excellent agreement is obtained.

In spite of the low anomalous collision frequencies, the turbulence levels in these simulations are quite high. Root mean square density fluctuations as high as 0.25 are seen. Although an expansion of the turbulence in plane waves predicts many of the observed effects, an expansion in terms of nonlinear waves, such as ion acoustic solitons, might prove superior.

In constant-current, $B=0$ simulations there is a characteristic shape for the electron distribution which is different from a drifting Maxwellian. The simulations discussed here were initialized with drifting Maxwellians in such a way that the unstable spectrum was optimally located in the k space available. When the electron distribution deformed into the "differential mobility" distribution, the location of the unstable spectrum was no longer optimal. Late time results are therefore questionable.

In future work we plan to reevaluate the T_e/T_i scaling and the V_d/V_{Te} scaling to check the conclusions presented here. The unstable spectrum for "differential mobility" distributions will be calculated, and such distributions will be used in these simulations.

REFERENCES

1. O. Buneman, *Phys. Rev. Lett.* **1**:8 (1958).
2. J. P. Boris, J. M. Dawson, J. H. Orens, and K. V. Roberts, *Phys. Rev. Lett.* **25**:706 (1970).
3. R. L. Morse and C. W. Nielson, *Phys. Rev. Lett.* **26**:3 (1971).
4. D. Biskamp and R. Chodura, *Phys. Rev. Lett.* **27**:1553 (1971).
5. D. Biskamp and R. Chodura, *Plasma Physics and Controlled Nuclear Fusion Research*, Vol. 2, (IAEA, Vienna, 1971), p. 265.
6. M. Lampe, W. M. Manheimer, J. B. McBride, J. H. Orens, K. Papadopoulos, R. Shanny, and R. N. Sudan, *Phys. Fluids* **15**:662 (1972).
7. D. Biskamp, K. U. von Hagenow, and H. Welter, *Phys. Lett.* **39A**:351 (1972).
8. J. A. Wesson, A. Sykes, and H. R. Lewis, *Plasma Phys.* **15**:49 (1973).
9. D. Biskamp and R. Chodura, **16**:893 (1973).
10. C. T. Dum, R. Chodura, and D. Biskamp, *Phys. Rev. Lett.* **32**:1231 (1974).
11. E. L. Lindman, *J. Phys. (Paris)* **38**:9 (1977) (Colloque C6).
12. J. S. DeGroot, C. Barnes, A. E. Walstead, and O. Buneman, *Phys. Rev. Lett.* **22**:1283 (1977).
13. J. M. Kindel, C. Barnes, and D. W. Forslund, in *Physics of Auroral Arc Formation*, Geophysical Monograph Series No. 25 (American Geophysical Union), p. 296.
14. C. Barnes, M. K. Hudson, and W. Lotko, *Phys. Fluids* (to be published).
15. C. K. Birdsall and D. Fuss, *J. Comput. Phys.* **3**:494 (1969); R. L. Morse and C. W. Nielson, *Phys. Fluids* **12**:2418 (1969); R. W. Hockney and J. W. Eastwood, *Computer Simulation Using particles* (McGraw-Hill, New York, 1981).
16. M. G. Haines, *Report of [1979] Workshop on "Transport of Fast Electrons in Laser-Fusion Plasmas"* (Centre Europeen de Calcul Atomique et Moleculaire, Orsay, France, 1981), p. 116.
17. R. C. Malone, R. L. McCrory, and R. L. Morse, *Phys. Rev. Lett.* **34**:721 (1975).
18. W. Horton, Jr., and Duk-In Choi, *Phys. Rep.* **49**:273 (1979).
19. H. Okuda and C. K. Birdsall, *Phys. Fluids* **13**:2123 (1970).
20. I. P. Shkarofsky, T. W. Johnson, and M. P. Bachynski, *The Particle Kinetics of Plasmas* (Addison Wells, Don Mills, Ontario), Chap. 3.
21. M. Abramowitz and I. Stegun, *Handbook of Mathematical Functions* (Dover Publications, New York, 19), Chap. 13.